

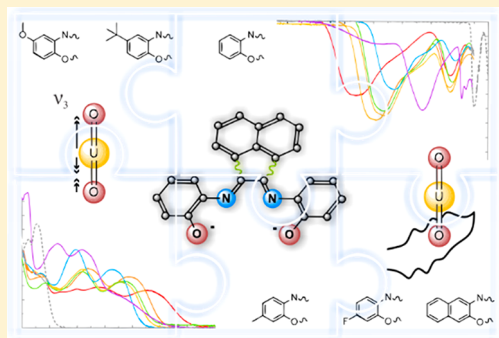
Bonding Interactions in Uranyl α -Diimine Complexes: A Spectroscopic and Electrochemical Study of the Impacts of Ligand Electronics and Extended Conjugation

Julie E. Niklas, Katherine M. Hunter, and Anne E. V. Gorden*[✉]

Department of Chemistry and Biochemistry, Auburn University, 179 Chemistry Building, Auburn, Alabama 36849, United States

Supporting Information

ABSTRACT: Uranyl complexes of aryl-substituted α -diimine ligands gbha ($\text{UO}_2\text{-1a-f}$) and phen-BIAN ($\text{UO}_2\text{-2a-f}$) [gbha (1) = glyoxal bis(2-hydroxyanil); phen-BIAN (2) = *N,N'*-bis(iminophenol)acenaphthene; R = OMe (a), *t*-bu (b), H (c), Me (d), F (e), and naphthyl (f)] were designed, prepared, and characterized by X-ray diffraction, FT-IR, NMR, UV–vis, and electrochemical methods. These ligand frameworks contain a salen-type O–N–N–O binding pocket but are redox-noninnocent, leading to unusual metal complex behaviors. Here, we describe three solid-state structures of uranyl complexes $\text{UO}_2\text{-1b}$, $\text{UO}_2\text{-1c}$, and $\text{UO}_2\text{-1f}$ and observe manifestations of ligand noninnocence for the U(VI) complexes $\text{UO}_2\text{-1b}$ and $\text{UO}_2\text{-1c}$. The impacts of accessible π -systems and ligand substitution on the axial uranium–oxo interactions were evaluated spectroscopically via the intra-ligand charge-transfer (ILCT) processes that dominate the absorption spectra of these complexes and through changes to the asymmetric (ν_3) O=U=O stretching frequency. This, in combination with electrochemical data, reveals the effects of the inclusion of the conjugated acenaphthene backbone and the importance of ligand electronic structure on uranyl's bonding interactions.



INTRODUCTION

The robust nature of the linear uranyl dication ($\text{O}=\text{U}=\text{O}^{2+}$) poses a unique challenge with respect to its activation and functionalization. The axial oxo ligands are covalently bound to the uranium center and mutually reinforce one another via the inverse-*trans*-influence (ITI), which distinguishes high-valent actinyl species from their transition metal counterparts.^{1–3} Recent efforts have focused on understanding the mechanisms by which this moiety can be reduced through the axial oxo ligands with particular interest in perturbation of their bonding character.^{4–9} The reduction of uranyl is of interest in developing our understanding of bioremediation, as some bacteria have been found to reduce the highly water-soluble uranyl (UO_2^{2+}) (U^{VI}) species to the insoluble U^{IV} species through a U^{V} intermediate via the oxo groups; however, this mechanism is not as yet well understood.¹⁰ U^{V} species are unstable due to disproportionation to the more stable U^{VI} and U^{IV} species; thus, characterization of systems in which the $\text{U}^{\text{VI/V}}$ redox couple can be studied or tuned is pertinent, especially where judicious choice of equatorial ligand may assist in the reduction or stabilization of lower-valent uranium centers. π -Bonded ligands, particularly those containing a significant accessible π -system, have been identified as being especially valuable in stabilizing through delocalization formally reduced uranium centers which behave as synthetic equivalents of low-valent species.¹¹

Redox-active frameworks have long been prevalent in transition metal systems but have only recently been utilized

for the characterization of uranium (in particular, uranyl) complexes.^{12–14} Participation of the ligand in redox processes and an inherent ability to stabilize atypical metal oxidation states is of interest.¹⁵ Pyridine(diimine) (PDI) ligands are known to assist in U=O bond scission⁶ and have been found to stabilize reduced species through π -backbonding interactions with uranium.¹⁶ Arnold and coworkers achieved activation and functionalization of the uranyl oxo ligands through sterically forced metal cation–oxo interactions in macrocyclic systems¹⁷ as well as the reduction of uranyl to U(IV) assisted by a redox-active donor-expanded dipyrin ligand.¹⁸ The study of systems that can both behave noninnocently and can participate in π -backbonding is of interest in evaluating covalent interactions and reduction processes. Such π -backbonding interactions are typically only discussed for more electron-rich actinide centers,^{11,16,19,20} not closed-shell systems such as UO_2^{2+} ; however, during the review period of this article, Liddle and coworkers demonstrated backbonding between an electron-poor U(V) center and dinitrogen, an especially poor π -acceptor.²¹ This is attributed to a suitably electron-rich ligand environment capable of providing the necessary electron density for backbonding. The electronic structure and bonding behaviors of actinides are still being explored, hence it is worth considering some of these behaviors may be less obvious or may be exhibited in a

Received: June 10, 2019

nonclassical way. Toward this end, we focused on redox-noninnocent α -diimine ligands and recently reported a new system, “phen-BIAN”,²² which features both an α -diimine fragment joined to a naphthalene unit, as found in Ar-BIANs,^{23,24} and the characteristic O–N–N–O binding pocket of salens, thereby extending the range of available ligand oxidation states (Figure 1). The complex [UO₂(*t*-bu)phen-

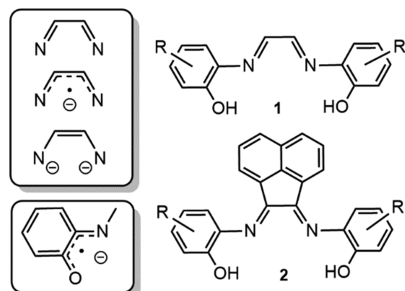


Figure 1. Idealized or “open” α -diimine ligands **1** (glyoxal-bis(2-hydroxyanil)) and **2** (phen-BIAN) used in this study (right) and possible redox states of the O–N–N–O pocket (left).

BIAN]₂ exhibited a surprising range of electrochemical behavior and engaged in oxo–solvent interactions in the solid-state,²² prompting us to pursue further study of complexes of this type. Additionally, we reported a uranyl complex of naphthylsalophen, which demonstrated significant metal–ligand communication as a result of the conjugated framework.²⁵ The properties of these two uranyl complexes inspired a combined study of the efficacy of the conjugated BIAN-type backbone as it compares to the inclusion of conjugated ligand donor-arms. To accomplish this, we prepared and studied five new derivatives of uranyl phen-BIAN complexes as well as a set of six derivatives of uranyl complexes of the analogous glyoxal-bis(2-hydroxyanil) (gbha) ligand, which lack the acenaphthene backbone of phen-BIANs.

Glyoxal-bis(2-hydroxyanils) function as tetradentate diphenolate ligands and have been used in colorimetric Ca²⁺ sensors.²⁶ These were also reported in work by Wilson from 1962 for potential use in the detection of trace quantities of metal ions in solution, including uranyl.^{27,28} Transition metal complexes of gbhas have not been widely characterized due to their low stability in addition to the poor solubility of both the free ligands and their complexes, which serves to limit the acquisition of solution-state data and often precludes crystallization.^{29,30} There are two reports of structurally characterized uranyl complexes of gbha, showing this complex can exist as a water coordinated monomer ([UO₂(gbha)(H₂O)]) or as a μ -phenolato bridged dimer ([UO₂(gbha)]₂).^{15,31} As a further complicating factor, the free, uncomplexed ligands exist primarily in their benzoxazinobenzoxazine forms, which has been frequently misassigned in the literature as a bisbenzoxazoline or as the open *trans* glyoxal-bis(hydroxyanil) form (Figure 2).^{32–34}

Only the unsubstituted gbha (5a,6,11a,12-tetrahydro[1,4]-benzoxazino[3,2-*b*][1,4]benzoxazine) has been previously characterized by X-ray diffraction.³² Here, we present three new gbha ligands (-OMe, -F, and -naphthyl-substituted) in addition to the crystal structure of *t*-bu-gbha and six new uranyl complexes of these ligands (R = OMe, *t*-bu, H, Me, F, 3-naphthyl), four of which have been characterized in the solid-state by single crystal X-ray diffraction. We describe these six

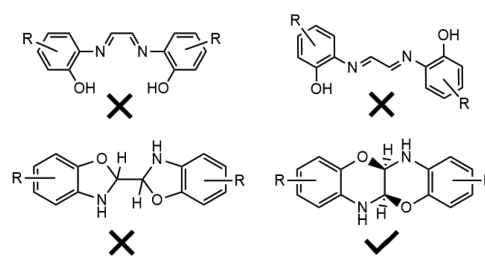


Figure 2. Reported forms of gbha ligands.

complexes alongside their phen-BIAN analogues with special attention to how the ligand substituents, especially the presence of accessible π -systems, impact their absorption spectra, ν_3 O=U=O stretching frequencies, and electrochemical behaviors.

EXPERIMENTAL METHODS

General Considerations. Caution! The uranium metal salt used in this study, UO₂(OAc)₂·2H₂O, contained depleted uranium. Standard precautions for handling radioactive materials or heavy metals such as uranyl nitrate and lead sulfate were followed. Organic solvents (EtOH, Pharmco-Aaper; MeOH, anhydrous THF (DriSolv), EMD Millipore; CH₂Cl₂, CHCl₃, acetone, THF, EtOAc, heptane, BDH Chemicals; benzene, Fisher Scientific; *n*-pentane, Acros Organics) were used as received without additional purification. Acenaphthenequinone, 2-amino-4-*tert*-butylphenol, 3-amino-2-naphthol, 2-amino-4-methoxyphenol, anhydrous ZnCl₂ (Alfa Aesar), *o*-aminophenol, chlorotrimethylsilane (Acros Organics), 2-amino-5-methylphenol, 2-amino-5-fluorophenol (Ark Pharm), and Et₃N (BDH Chemicals) were used as received. TBAPF₆ (Beantown Chemical) was recrystallized from anhydrous EtOH, and uranyl acetate (Polysciences) was recrystallized from methanol prior to use. ¹H and ¹³C NMR were recorded on a Bruker AV 400 or 600 MHz spectrometer using DMSO-*d*₆, DMF-*d*₇, or CDCl₃ (Cambridge Isotope Laboratories) as indicated. Chemical shifts are reported in parts per million (δ) and referenced against residual internal solvent signals. Purity of compounds was established via NMR and elemental analysis or mass spectrometry (TOF MS, ES+). Elemental analyses were performed by Atlantic Microlab, Inc. UV/vis data were collected on a Varian Cary 50 WinUV spectrophotometer. Infrared spectra were obtained in the solid state using an attenuated total reflectance (ATR) method on a Thermo Scientific Nicolet iS50 FT-IR, and spectra were normalized [0, 100] using OriginPro.

X-ray Crystallography. Crystals suitable for single crystal X-ray diffraction were selected and mounted on a 50- μ m MiTeGen loop using Paratone-N oil, and data set collection was completed on a Bruker D8 VENTURE κ -geometry diffractometer using Cu K α radiation (Incoatec I μ S DIAMOND microfocussed tube, λ = 1.54178 Å). Crystals were kept at 100 K (150 K for UO₂-1e) during unit cell and data collection. Determination of the unit cell and collection of data were performed using the APEX III software, and determination of integrated intensities and global cell refinement were performed with the Bruker SAINT software package. An empirical absorption correction (SADABS) was applied. Structures were solved using Intrinsic Phasing/Direct Methods^{35,36} (ShelXT), and least-squares refinement was performed using ShelXL in APEX III. Olex2.1³⁷ was used to mask solvent molecules (UO₂-1c) to achieve convergence. Restraints and constraints such as FLAT, SIMU, ISOR, and EADP were employed for atoms that would otherwise be split and could not be modeled over two positions due to unresolved twinning or for atoms that could not be refined anisotropically without resulting in nonpositive definites. Projections were created on Olex2.1.

Computational Methods. All electronic structure calculations were performed in the Gaussian 16 suite³⁸ using the B3LYP functional and 6-31G(d) basis set. Atom coordinates were adapted from the asymmetric unit of UO₂-1b after removing the central UO₂²⁺

fragment and adding aryl substituents in Avogadro v1.2.0.³⁹ The binding pocket atoms (O–C–C–N–C–C–O) were held rigid, and all remaining atoms' geometries were optimized. Molecular orbitals were visualized in Avogadro.

Electrochemical Measurements. Electrochemical measurements were carried out using a CH Instruments 660 E potentiostat in HPLC-grade CH₂Cl₂ (BDH Chemicals) with tetrabutylammonium hexafluorophosphate (TBAPF₆) supporting electrolyte (0.1 M). TBAPF₆ was recrystallized from EtOH and dried overnight in vacuo at 60 °C immediately before use. Solutions were purged for 30 min with N₂ using a prepurge solution. Potentials were scanned using a three-electrode cell consisting of a glassy carbon disc working electrode, Pt wire counter electrode, and Ag/AgCl/satd. KCl/H₂O reference electrode. Data were corrected versus ferrocene based on values for E_{1/2}(Fc/Fc⁺) collected using the same three-electrode cell before and after measurements. DPV conditions: increment: 0.01 V; amplitude: 0.05 V; pulse width: 0.05 s; sample width: 0.0167 s; pulse period: 0.5 s.

Synthesis of OMe-gbha (1a). A solution of glyoxal (40% w/w aq., 0.11 mL, 1.0 mmol) in methanol (5 mL) was heated to 65 °C in a 250 mL round-bottom flask while being stirred. 2-Amino-4-methoxyphenol (0.278 g, 2.0 mmol) was dissolved in methanol (5 mL) and added to the solution. Then, one drop of glacial acetic acid was added. A precipitate formed within several minutes, and the solution was heated and stirred at reflux temperature for 3 h. After being allowed to cool to room temperature, a mustard-yellow product was collected by filtration and rinsed with methanol. Yield: 0.153 g, 55.0%. ¹H NMR (400 MHz, DMSO-*d*₆): δ 7.27 (s, 2H), 6.56 (d, 2H, *J* = 8.55), 6.26 (s, 2H), 6.18 (d, 2H, *J* = 8.53), 5.13 (s, 2H), 3.64 (s, 6H). ¹³C NMR (600 MHz, DMSO-*d*₆): δ 154.25, 135.11, 130.90, 116.28, 103.34, 99.86, 75.16, 55.15. FT-IR (ATR): 3374 cm⁻¹ (N–H). λ_{max}: 305 nm (10 363 M⁻¹ cm⁻¹). HRMS (ESI+) *m/z* [M + 1] calcd 301.1188, found 301.1187.

Synthesis of *t*bu-gbha (1b). A solution of glyoxal (40% w/w aq., 0.58 mL, 5 mmol) in methanol (5 mL) with one drop of glacial acetic acid was heated to 65 °C in a 250 mL round-bottom flask with stirring. To this solution, 2 equiv of 2-amino-4-*tert*-butylphenol (1.65 g, 10 mmol) in hot methanol (45 mL) was added, and the resulting brown solution was heated and stirred at reflux temperature for 1 h. The resulting white precipitate was collected via vacuum filtration and rinsed with methanol. The filtrate was concentrated using a rotary evaporator and placed in the freezer overnight, yielding additional product. Yield: 1.25 g, 71%. Single crystals suitable for X-ray diffraction were grown from a concentrated solution of CDCl₃. ¹H NMR (400 MHz, CDCl₃): δ 6.79 (dd, 2H, *J* = 8.48, 2.08), 6.74 (d, 2H, *J* = 8.40), 6.71 (d, 2H, *J* = 1.72), 5.29 (d, 2H, *J* = 3.6 Hz), 4.85 (d, 2H, *J* = 3.6 Hz), 1.27 (s, 18H). ¹³C NMR (400 MHz, CDCl₃): 145.14, 139.12, 127.73, 117.56, 116.55, 112.17, 76.12, 34.19, 31.49. FT-IR(ATR): 3372 cm⁻¹ (N–H). λ_{max}: 298 nm (11 823 M⁻¹ cm⁻¹). HRMS (ESI+) *m/z* [M + 1] calcd 353.2229, found 353.2222.

Synthesis of gbha (1c). A solution of glyoxal (40% w/w aq., 0.58 mL, 5 mmol) in methanol (5 mL) with one drop of glacial acetic acid was heated to 65 °C in a 250 mL round-bottom flask with stirring. To this solution, 2 equiv of *o*-aminophenol (1.09 g, 10 mmol) in hot MeOH (45 mL) was added, and the resulting brown solution was heated and stirred at reflux temperature for 1 h. A pale purple crystalline precipitate formed and was collected by vacuum filtration and rinsed with MeOH. The filtrate was concentrated using a rotary evaporator and placed in the freezer to yield additional product. Yield: 0.120 g, 50%. ¹H NMR (400 MHz, DMF-*d*₇): δ 7.34 (d, 2H, *J* = 3.88), 6.80 (m, 4H), 6.68 (m, 4H), 5.38 (d, 2H, *J* = 4.12). ¹³C NMR (400 MHz, DMF-*d*₇): δ 142.94, 131.60, 122.44, 119.86, 117.26, 115.44, 77.02. FT-IR(ATR): 3370, 3379 cm⁻¹ (N–H). λ_{max}: 286 nm (8097 M⁻¹ cm⁻¹). HRMS (ESI+) *m/z* [M + 1] calcd 241.0977, found 241.0977.

Synthesis of Me-gbha (1d). A solution of glyoxal (40% w/w aq., 0.58 mL, 5.0 mmol) in methanol (5 mL) with one drop of glacial acetic acid was heated to 65 °C in a 250 mL round-bottom flask with stirring. To this solution, 2-amino-5-methylphenol (1.23 g, 10 mmol) in hot methanol (45 mL) was added, and the resulting brown solution

was heated and stirred at reflux temperature for 1.5 h. The resulting white precipitate was collected via vacuum filtration and rinsed with methanol. Yield: 1.04 g, 77.0%. ¹H NMR (400 MHz, DMSO-*d*₆): δ 7.11 (d, 2H, *J* = 4.01), 6.55 (m, 4H), 6.46 (s, 2H), 5.20 (d, 2H, *J* = 3.98), 2.12 (s, 6H). ¹³C NMR (600 MHz, DMSO-*d*₆): δ 141.31, 127.53, 127.49, 121.66, 116.49, 114.07, 75.48, 20.28. FT-IR (ATR): 3371 cm⁻¹ (N–H). λ_{max}: 301 (12 377 M⁻¹ cm⁻¹). HRMS (ESI+) *m/z* [M + Na⁺] calcd 277.0793, found 291.1109.

Synthesis of F-gbha (1e). A solution of glyoxal (40% w/w aq., 0.11 mL, 2.0 mmol) in methanol (5 mL) was heated to 65 °C in a 100 mL round-bottom flask while being stirred. To this solution, 2-amino-5-fluorophenol (0.278 g, 2 mmol) dissolved in methanol (10 mL) was added, and then one drop of glacial acetic acid was added. A precipitate formed within several minutes, and the solution was heated and stirred at reflux temperature for 6 h. After cooling to room temperature, a brown crystalline solid was collected by filtration and rinsed with methanol. The filtrate was concentrated using a rotary evaporator and placed in the freezer for several weeks, yielding a small amount of additional product. Yield: 0.047 g, 17.1%. ¹H NMR (400 MHz, DMSO-*d*₆): δ 7.31 (s, 2H), 6.66 (m, 2H), 6.58 (m, 4H), 5.33 (s, 2H). ¹³C NMR (600 MHz, DMSO-*d*₆): δ 156.42, 154.87, 142.01 (d), 126.43 (d), 114.30 (d), 107.40 (d), 103.55 (d), 75.426. FT-IR (ATR): 3364 cm⁻¹ (N–H). λ_{max}: 302 nm (10 187 M⁻¹ cm⁻¹). HRMS (ESI+) *m/z* [M + 1] calcd 277.0789, found 277.0793.

Synthesis of 3N-gbha (1f). A solution of 3-amino-2-naphthol (0.160 g, 1.00 mmol) in methanol (25 mL) was heated to reflux temperature 65 °C in a 100 mL round-bottom flask until it completely dissolved. Glyoxal (40% w/w aq., 0.11 mL, 1.00 mmol) was diluted to ~5 mL in deionized water, and 4 drops glacial acetic acid were added. The glyoxal solution was added dropwise to the 3-amino-2-naphthol solution over 7 min, during which time a light precipitate formed. The mixture was stirred and heated for an additional 5 min and then cooled to room temperature, and the pearlescent tan solid produced was collected by vacuum filtration and rinsed with MeOH. Yield: 0.085 g, 25.0%. ¹H NMR (400 MHz, DMSO-*d*₆): δ 7.93 (s, 2H), 7.59 (t, 4H, *J* = 9.28), 7.22 (m, 4H), 7.07 (s, 2H), 5.49 (s, 2H). ¹³C NMR (600 MHz, DMSO-*d*₆): δ 143.31, 130.95, 129.88, 128.09, 126.17, 125.34, 123.90, 122.62, 111.18, 108.07, 75.49. FT-IR(ATR): 3403 cm⁻¹ (N–H). λ_{max}: 342 nm (22 594 M⁻¹ cm⁻¹). HRMS (ESI+) *m/z* [M + 1] calcd 341.1283, found 341.1290.

Synthesis of gbha complexes. For the R-gbha (R = H, Me, *t*-bu, OMe), the complexes were synthesized by direct addition of the gbha ligand to the metal salt. The fluoro- and 3N- complexes were synthesized by templation due to the low yield (F-) and poor solubility (3N-) of the free ligands.

Synthesis of UO₂-1a. A methanolic solution (20 mL) of OMe-gbha (0.061 g, 0.20 mmol) was heated to 65 °C in a 100 mL round-bottom flask and stirred until dissolved. UO₂(OAc)₂·2H₂O (0.084 g, 0.20 mmol) was dissolved in a minimum amount of methanol and added to the ligand solution, which turned dark green. The reaction mixture was stirred and heated for 4.5 h and then cooled to room temperature and stored in the freezer overnight. A dark solid was collected by filtration. Yield: 0.065 g, 57.2%. ¹H NMR (400 MHz, DMSO-*d*₆): δ 7.43 (s, 2H), 7.15 (d, 2H, *J* = 9.08), 6.76 (d, 2H, *J* = 8.95), 3.83 (s, 2H). ¹³C NMR (600 MHz, DMSO-*d*₆): δ 168.51, 151.74, 150.74, 138.24, 123.14, 121.51, 91.72, 55.90. FT-IR (ATR): 924, 909 cm⁻¹ (O=U=O, ν₃). λ_{max}¹: 709 nm (10 301 M⁻¹ cm⁻¹). HRMS (ESI+) *m/z* [M + Na] calcd 1159.2617, found 1159.2583.

Synthesis of UO₂-1b. A methanolic solution (45 mL) of *t*bu-gbha (0.141 g, 0.4 mmol) was heated to 65 °C in a 250 mL round-bottom flask and stirred until dissolved. UO₂(OAc)₂·2H₂O (0.170 g, 0.4 mmol) was dissolved in a minimum amount of hot methanol and added to the solution. The resulting blue-green solution was stirred at reflux temperature for 4 h, yielding a dark precipitate. The solution was cooled to room temperature and then stored in the freezer overnight. A dark bronze precipitate was collected via vacuum filtration (yield: 0.215 g, 72%). Red-purple crystals suitable for X-ray diffraction were grown from a concentrated acetone solution in a small test tube inside a sealed vial containing pentane. ¹H NMR (400 MHz, DMSO-*d*₆): δ 9.43 (s, 2H), 7.83 (d, 2H, *J* = 2.28), 7.55 (dd,

2H, $J = 8.92, 2.28$), 6.76 (d, 2H, $J = 8.76$), 1.36 (s, 18H). ^{13}C NMR (600 MHz, DMSO- d_6): δ 171.05, 151.33, 139.97, 137.82, 131.55, 120.35, 113.29, 34.17, 31.42. FT-IR (ATR): 921 cm^{-1} (O=U=O, ν_3). $\lambda_{\text{max}}^{-1}$: 648 nm (12 634 $\text{M}^{-1} \text{cm}^{-1}$). HRMS (ESI+) m/z [$M + 1$] calcd 1241.4879, found 1241.4877.

Synthesis of $\text{UO}_2\text{-1c}$. A methanolic solution of gbha (0.057 g, 0.23 mmol) was heated to 65 °C in a 100 mL round-bottom flask and stirred until dissolved. $\text{UO}_2(\text{OAc})_2 \cdot 2\text{H}_2\text{O}$ (0.100 g, 0.23 mmol) was dissolved in a minimum amount of hot methanol and added to the solution. The resulting dark blue solution was stirred at reflux temperature for 3 h, yielding a dark precipitate. The solution was cooled to room temperature, and a dark green solid was collected by filtration. Yield: 0.068 g, 58.2%. Single crystals suitable for X-ray diffraction were grown by vapor diffusion in a CH_2Cl_2 solution inside a vial of methanol. ^1H NMR (400 MHz, DMSO- d_6): δ 9.41 (s, 2H), 7.93 (d, 2H, $J = 9.60$), 7.46 (t, 2H, $J = 4.46$), 6.81 (m, 4H). ^{13}C NMR (600 MHz, DMSO- d_6): δ 173.44, 152.76, 139.17, 134.43, 121.53, 118.00, 117.75. FT-IR (ATR): 913, 904 cm^{-1} (O=U=O, ν_3). $\lambda_{\text{max}}^{-1}$: 660 nm (6500 $\text{M}^{-1} \text{cm}^{-1}$). HRMS (ESI+) m/z [$M + 1$] calcd 509.1227, found 509.1226.

Synthesis of $\text{UO}_2\text{-1d}$. A methanolic solution (40 mL) of Me-gbha (0.187 g, 0.7 mmol) was heated to 65 °C in a 250 mL round-bottom flask and stirred until dissolved. $\text{UO}_2(\text{OAc})_2 \cdot 2\text{H}_2\text{O}$ (0.297 g, 0.7 mmol) was dissolved in a minimum amount of hot methanol and added to the solution, which turned dark blue. The reaction mixture was stirred at reflux temperature for 2 h, producing a dark precipitate, which then was cooled to room temperature. A dark green solid was collected by filtration. Yield: 0.362 g, 96.0%. ^1H NMR (400 MHz, DMSO- d_6): δ 9.30 (s, 2H), 7.78, d, 2H, $J = 8.36$), 6.62 (m, 4H), 2.35 (s, 6H). ^{13}C NMR (600 MHz, DMSO- d_6): δ 150.78, 144.30, 136.79, 121.00, 118.73, 116.99, 21.65. FT-IR (ATR): 915 cm^{-1} (O=U=O, ν_3). $\lambda_{\text{max}}^{-1}$: 613 nm (13 073 $\text{M}^{-1} \text{cm}^{-1}$). HRMS (ESI+) m/z [$M + 1$] calcd 537.1540, found 537.1531.

Synthesis of $\text{UO}_2\text{-1e}$. A solution of glyoxal (40% w/w aq., 0.06 mL, 0.5 mmol) in methanol (5 mL) was heated to 65 °C with stirring. $\text{UO}_2(\text{OAc})_2 \cdot 2\text{H}_2\text{O}$ (0.212 g, 0.5 mmol) was dissolved in a minimum amount of hot methanol and added to the solution. 2-Amino-5-fluorophenol (0.127 g, 1.00 mmol) was dissolved in ~20 mL of hot methanol and added to the reaction mixture, resulting in a dark purple solution and formation of a dark precipitate. The solution was heated and stirred for 5 h and then cooled to room temperature, and the dark solid was collected by filtration. Yield: 0.164 g, 60.2%. Single crystals suitable for X-ray diffraction were grown by vapor diffusion from a THF solution inside a vial of pentane. ^1H NMR: δ 8.40 (s, 2H), 7.99 (t, 2H, $J = 7.42$), 6.67 (m, 2H). ^{13}C NMR (600 MHz, DMSO- d_6): δ 174.15 (d), 167.78, 166.12, 152.72, 136.05, 118.77, 106.77, 104.95. FT-IR (ATR): 919 cm^{-1} (O=U=O, ν_3). $\lambda_{\text{max}}^{-1}$: 575 nm (9542 $\text{M}^{-1} \text{cm}^{-1}$). HRMS (ESI+) m/z [$M + \text{Na}$] calcd 1111.1818, found 1111.1838.

Attempted Synthesis of $\text{UO}_2\text{-1f}$. Several methods of synthesizing $\text{UO}_2\text{-1f}$ were employed to acquire pure product; however, the poor solubility of both the ligand (and stability of the cyclic form) and the complex precludes their separation. Reaction of the ligand with uranyl acetate in hot methanol either with or without base, in an 80:20 THF:methanol mixture with base, and by templation in methanol with and without base each yielded a dark brown product which, by NMR, contains a 50:50 mixture of the metal complex and ligand. Attempts to separate the ligand from the complex with a variety of solvent systems (including THF, THF/methanol mixtures, hexanes, and dichloromethane) were unsuccessful. After these attempts, a reduction in the ligand peaks was not observed by NMR; hence, the complex may be unstable in solution. We were able to obtain a single crystal of the product by crystallization from a benzene/methanol mixture and pentane to confirm its identity. FT-IR (ATR): 917, 910 (O=U=O, ν_3). $\lambda_{\text{max}}^{-1}$: ~640 nm (~4600–4900 $\text{M}^{-1} \text{cm}^{-1}$). HRMS (ESI+) m/z [$M + 1$] calcd 609.1540, found 609.1540.

Synthesis of Phen-BIAN Complexes. The complex $\text{UO}_2\text{-2b}$ was synthesized according to the previously published procedure.²² The other phen-BIAN complexes were synthesized by templation of the substituted ligand around uranyl. Protection of the alcohol with TMS

groups was required to prepare the H and naphthyl derivatives ($\text{UO}_2\text{-2c}$ and $\text{UO}_2\text{-2f}$).

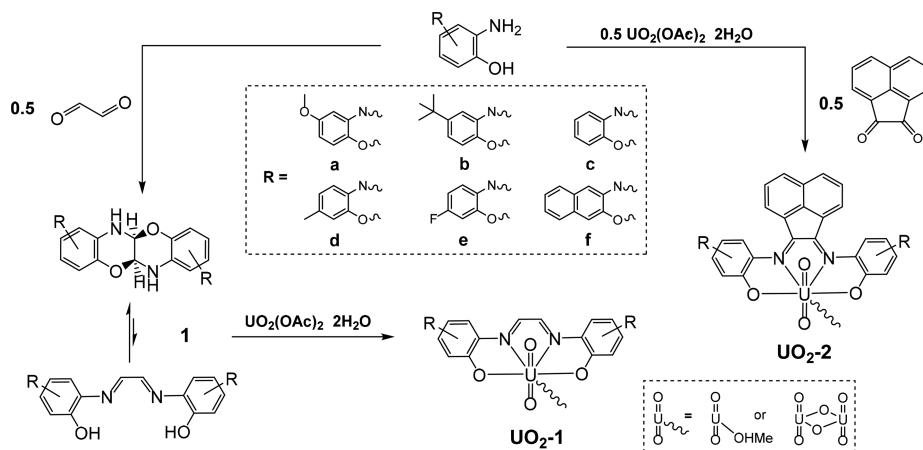
Synthesis of $\text{UO}_2\text{-2a}$. Acenaphthenequinone (0.091g, 0.50 mmol) was added to a 100 mL round-bottom flask charged with a stir bar and heated to 68 °C in methanol (40 mL) with stirring until completely dissolved. 2-Amino-4-methoxyphenol (0.139 g, 1.0 mmol) and $\text{UO}_2(\text{OAc})_2 \cdot 2\text{H}_2\text{O}$ (0.212 g, 0.5 mmol) were added as solids, and the flask was rinsed with an additional 5 mL of methanol. The solution turned black within 10 min and was heated and stirred for 24 h, producing a black precipitate. After the solution was cooled to room temperature, a small quantity of fine, black powder was collected by filtration and rinsed with copious amounts of methanol. Attempts to isolate additional product by concentrating the filtrate and storing it in the freezer were unsuccessful. Yield: 0.064 g, 18.5%. ^1H NMR: δ 8.81 (d, 2H, $J = 7.28$), 8.32 (d, 2H, $J = 8.28$), 7.93 (t, 2H, $J = 7.85$), 7.59 (d, 2H, $J = 2.59$), 7.17 (dd, 2H, $J = 8.98, 2.75$), 6.83 (d, 2H, $J = 9.80$), 3.82 (s, 6H). FT-IR (ATR): 909 cm^{-1} (O=U=O, ν_3). $\lambda_{\text{max}}^{-1}$: 753 nm (5398 $\text{M}^{-1} \text{cm}^{-1}$). Anal. calcd for $\text{C}_{78}\text{H}_{54}\text{N}_6\text{O}_{18}\text{U}_3 \cdot \text{H}_2\text{O}$: C, 44.71; H, 2.69; N, 4.01. Found: C, 44.71; H, 2.84; N, 4.09.

Synthesis of $\text{UO}_2\text{-2c}$. The synthesis of *o*-trimethylsilyl-2-amino-phenol was adapted from a published procedure.⁴⁰ In a 50 mL round-bottom flask, *o*-aminophenol (0.437 g, 4.0 mmol) was stirred at room temperature in dichloromethane (5 mL). Chlorotrimethylsilane (0.51 mL, 4.0 mmol) and triethylamine (0.56 mL, 4.0 mmol) were added; the mixture was stirred for 18 h, and the solvent was removed using a rotary evaporator. The product was extracted into pentane and filtered over a short pad of Celite to remove the triethylamine salt and then dried to an orange oil which crystallized below room temperature. Yield: 0.583 g, 80.5%. ^1H NMR (400 MHz, CDCl_3): δ 6.83–6.74 (m, 3H), 6.65 (td, 1H, $J = 7.56, 1.60$), 0.32 (s, 9H). ^{13}C NMR (400 MHz, CDCl_3): 142.92, 138.35, 122.13, 118.69, 118.57, 115.81, 0.60.

Acenaphthenequinone (0.091 g, 0.5 mmol) was added to a 250 mL round-bottom flask charged with a stir bar and heated to 78 °C in ethanol (30 mL) with stirring until completely dissolved. *O*-Trimethylsilyl-2-aminophenol (0.181 g, 1.0 mmol) and $\text{UO}_2(\text{OAc})_2 \cdot 2\text{H}_2\text{O}$ (0.212 g, 0.5 mmol) were added, and the flask was rinsed with an additional 5 mL of ethanol. The reaction mixture turned golden-brown and was heated and stirred for 18 h, during which time it turned black. After the solution was cooled to room temperature, a fine, black powder was collected by filtration. Yield: 0.211 g, 67.0%. ^1H NMR (400 MHz, DMSO- d_6): δ 7.52 (d, 2H, $J = 7.42$), 7.17 (d, 2H, $J = 8.20$), 6.98 (d, 2H, 7.08), 6.81 (t, 2H, $J = 7.84$), 6.50 (t, 2H, $J = 8.28$), 6.01 (m, 4H). FT-IR (ATR): 907, 902 cm^{-1} (O=U=O, ν_3). $\lambda_{\text{max}}^{-1}$: 753 nm (5398 $\text{M}^{-1} \text{cm}^{-1}$). Anal. calcd for $\text{C}_{24}\text{H}_{14}\text{N}_2\text{O}_4\text{U} \cdot \text{Cl}$: C, 43.16; H, 2.11; N, 4.19. Found: C, 43.10; H, 2.23; N, 4.10.

Synthesis of $\text{UO}_2\text{-2d}$. Acenaphthenequinone (0.091g, 0.50 mmol) was added to a 250 mL round-bottom flask charged with a stir bar and heated to 68 °C in methanol (40 mL) with stirring until completely dissolved. 2-Amino-5-methylphenol (0.123 g, 1.0 mmol) and $\text{UO}_2(\text{OAc})_2 \cdot 2\text{H}_2\text{O}$ (0.212 g, 0.5 mmol) were added as solids, and the flask was rinsed with an additional 5 mL of methanol. The solution turned dark immediately and was heated and stirred for 1 h, producing purple precipitate. After the solution was cooled to room temperature, the purple-black solid was collected by filtration. Yield: 0.184 g, 55.7%. ^1H NMR (400 MHz, DMSO- d_6): δ 8.78 (d, 2H, $J = 7.37$), 8.32 (d, 2H, $J = 8.19$), 7.98 (d, 2H, $J = 8.68$), 7.87 (t, 2H, $J = 7.82$), 6.70 (m, 4H), 4.11 (4, 2H, $J = 5.25$, MeOH), 3.17 (d, 6H, $J = 5.25$, MeOH), 2.39 (s, 6H). ^{13}C NMR (600 MHz, DMSO- d_6): δ 171.07, 160.22, 156.51, 143.20, 135.37, 131.34, 131.23, 128.33, 127.17, 123.20, 120.94, 120.60, 117.40, 21.76. FT-IR (ATR): 897 cm^{-1} (O=U=O, ν_3). $\lambda_{\text{max}}^{-1}$: 674 nm (6611 $\text{M}^{-1} \text{cm}^{-1}$). Anal. calcd for $\text{C}_{52}\text{H}_{36}\text{N}_4\text{O}_8\text{U}_2 \cdot 4(\text{H}_2\text{O})$: C, 44.84; H, 3.18; N, 4.02. Found: C, 44.86; H, 3.18; N, 4.00.

Synthesis of $\text{UO}_2\text{-2e}$. Acenaphthenequinone (0.063 g, 0.35 mmol) was added to a 100 mL round-bottom flask charged with a stir bar and heated to 68 °C in methanol (40 mL) with stirring until completely dissolved. 2-Amino-5-fluorophenol (0.102 g, 0.8 mmol) and $\text{UO}_2(\text{OAc})_2 \cdot 2\text{H}_2\text{O}$ (0.170 g, 0.40 mmol) were added as solids, and the flask was rinsed with an additional 5 mL of ethanol. The reaction

Scheme 1. General Synthesis of Gbha Ligands (**1**) and Uranyl Complexes $\text{UO}_2\text{-1}$ and $\text{UO}_2\text{-2}$ 

mixture was heated and stirred for 18 h, producing a black precipitate. After the solution was cooled to room temperature, a fine, black powder was collected by filtration. Yield: 0.180 g, 77.0%. $^1\text{H NMR}$: δ 8.75 (d, 2H, $J = 7.66$), 8.36 (d, 2H, $J = 8.35$), 8.14 (t, 2H, $J = 7.98$), 7.90 (t, 2H, $J = 7.38$), 6.72 (d, 4H, $J = 9.59$). FT-IR (ATR): 901 cm^{-1} ($\text{O}=\text{U}=\text{O}$, ν_3). $\lambda_{\text{max}}^{-1}$: 629 nm ($8339\text{ M}^{-1}\text{ cm}^{-1}$). Anal. calcd for $\text{C}_{48}\text{H}_{24}\text{F}_4\text{N}_4\text{O}_8\text{U}_2$: C, 43.13; H, 1.81; N, 4.19. Found: C, 43.18; H, 1.79; N, 4.20.

Synthesis of $\text{UO}_2\text{-2f}$. The synthesis of 2-trimethylsilyloxy-3-aminonaphthalene was adapted from the published procedure for the synthesis of *o*-trimethylsilyloxy-2-aminophenol.⁴⁰ In a 50 mL round-bottom flask, 3-amino-2-naphthol (0.159 g, 1.0 mmol) was stirred at room temperature in dichloromethane (5 mL). Chlorotrimethylsilane (0.13 mL, 1.0 mmol) and triethylamine (0.14 mL, 41.0 mmol) were added; the mixture was stirred for 18 h, and the solvent was removed using a rotary evaporator. The product was extracted into heptane, filtered over Celite to remove the triethylamine salt, and then dried to a red-orange oil which crystallized below room temperature. Yield: 0.220 g, 95.1%. $^1\text{H NMR}$ (400 MHz, CDCl_3): δ 7.58 (dd, 2H, $J = 8.2$, 2.8), 7.30–7.20 (m, 2H), 7.11 (s, 1H), 7.04 (s, 1H), 4.02 (bs, 2H), 0.39 (s, 9H). $^{13}\text{CNMR}$ (600 MHz, $\text{DMSO-}d_6$): δ 146.12, 138.52, 129.52, 127.38, 125.40, 124.53, 122.66, 121.17, 107.96, 106.65, 2.04, 1.84.

Acenaphthenequinone (0.073 g, 0.4 mmol) was added to a 250 mL round-bottom flask and heated to 78 °C in ethanol (40 mL) with stirring until completely dissolved. 2-Trimethylsilyloxy-3-aminonaphthalene (0.185 g, 0.8 mmol) and $\text{UO}_2(\text{OAc})_2\cdot 2\text{H}_2\text{O}$ (0.170 g, 0.4 mmol) were added, and the flask was rinsed with an additional 5 mL of ethanol. The reaction mixture was heated and stirred for 48 h. After the solution was cooled to room temperature, a black solid was collected by filtration. Yield: 0.244 g, 83.3%. $^1\text{H NMR}$: δ 8.90 (d, 2H, $J = 7.52$), 8.68 (s, 2H), 8.44 (d, 2H, $J = 8.18$), 7.93 (m, 4H), 7.72 (d, 2H, $J = 8.16$), 7.45 (t, 2H, $J = 7.55$), 7.23 (t, 2H, 7.21), 7.13 (s, 2H). FT-IR(ATR): 916 , 909 cm^{-1} ($\text{O}=\text{U}=\text{O}$, ν_3). $\lambda_{\text{max}}^{-1}$: $\sim 640\text{ nm}$ ($\sim 4600\text{--}4900\text{ M}^{-1}\text{ cm}^{-1}$). Anal. calcd for $\text{C}_{64}\text{H}_{36}\text{N}_4\text{O}_8\text{U}_2\cdot\text{H}_2\text{O}$: C: 51.83; H: 2.58; N: 3.78; Found: C: 52.11, H: 2.61, N 3.78.

RESULTS AND DISCUSSION

Synthesis and Structural Features. The gbha ligands **1a–f** were synthesized by means of the condensation of glyoxal and the corresponding aminophenol (Scheme 1). These species exist as cyclic benzoxazinobenzoxazines in solution and solid state as determined by NMR and IR spectroscopy. N–H stretches are apparent at $3364\text{--}3403\text{ cm}^{-1}$ (Figure S33); imine stretches are absent in the $1650\text{--}1700\text{ cm}^{-1}$ region, and both C–H and N–H protons can be identified in the $^1\text{H NMR}$ spectrum (Figures S5–16) Additionally, this assignment was confirmed by single-crystal X-ray diffraction analysis for **1b**

(Figure S36), which to our knowledge is only the second reported crystal structure of a free “gbha” ligand of this type.³² In protic solvents such as methanol, some of these ligands (most noticeably **1b**) exist in equilibrium with the open gbha form, as evidenced by the blue-purple color of the solution. These species react quickly with uranyl acetate, resulting in very intensely colored green, blue, and purple solutions and pearlescent nearly black solids. The uranyl complexes form either μ -phenolato bridged dimers or methanol-coordinated monomers.

The physicochemical data acquired for $\text{UO}_2\text{-1}$ and $\text{UO}_2\text{-2}$ suggest that the nuclearity of the complexes is solvent-dependent, and in the solid-state, the structure is impacted heavily by crystallization conditions. The analysis by $^1\text{H NMR}$ in DMSO consistently indicates a single coordination environment, and only in one case ($\text{UO}_2\text{-2d}$) was there indication of coordination by a methanol solvent molecule. Mass spectral analyses of the $\text{UO}_2\text{-1}$ complexes from a 2:1 $\text{CH}_3\text{CN}:\text{THF}$ solution indicate the presence of primarily the dimeric species, though electrochemical characterization attempted in both THF and CH_3CN indicates these complexes behave in an entirely different fashion, not consistent with a dinuclear, bridged complex, but rather as monomeric species (Figure S42).

The complex $\text{UO}_2\text{-1b}$ crystallizes in $\bar{P}1$ as the μ -phenolato-bridged dimer $[\text{UO}_2(t\text{-bu})\text{gbha}]_2$ with an interatomic U–U distance of 4.0143(9) Å. This is the same bonding motif observed for the analogous complex $[\text{UO}_2(t\text{-bu})\text{phenBIAN}]_2$.²² The complexes $\text{UO}_2\text{-1c}$ and $\text{UO}_2\text{-1f}$ are methanol-coordinated monomers in the solid-state and form pseudodimers through hydrogen bonding between the methanolic proton of one monomer and phenolic O atom of the next. These three complexes all engage in weak, long-range (2.4–2.8 Å) interactions between the uranyl oxo groups and adjacent hydrogen atoms (MeOH, imine H, and interstitial benzene) (Figures S38–40) The orientation of the oxo groups into these “proton pockets” is not unusual when taking into account packing and electrostatic forces; however, in the case of $\text{UO}_2\text{-1c}$, these can be considered a stabilizing force for the elongated U=O bond (1.809(9) Å). The $\text{UO}_2\text{-1c}$ complex is the only structure of this group which features significant uranyl–oxo bond elongation: $\text{UO}_2\text{-1b}$ and $\text{UO}_2\text{-1f}$ have average U=O bond lengths of 1.784(13) and 1.778(11) Å, respectively, with only slight asymmetry observed for $\text{UO}_2\text{-1f}$.

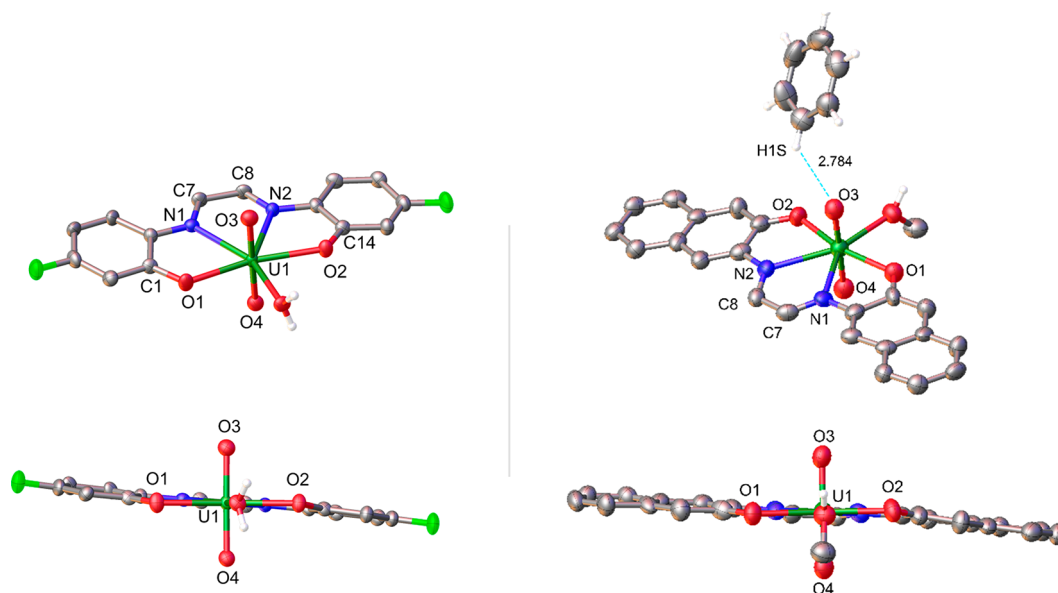


Figure 6. Left: Molecular structure and side-on view of asymmetric unit of $\text{UO}_2\text{-1e}$. Right: Molecular structure and side-on view of asymmetric unit of $\text{UO}_2\text{-1f}$. Select hydrogen atoms were omitted for clarity.

by 15.19° (N102, O102, C109–114) or 11.65° (N101, O101, C101–106). Deviation from planarity is observed for one ring in the water-coordinated complex $\text{UO}_2(\text{gbha})(\text{H}_2\text{O})$,³¹ but this is cited as a repulsive interaction between the ring and a nearby oxo ligand, and this is not observed for our system. Both units (Figure 5) have asymmetric and/or elongated uranyl oxo bonds (U1–O3:1.809(9) Å, U1–O4:1.776(11) Å; U101–O103:1.786(10) Å, U101–O104:1.797(15) Å); these are notable increases in length (nearly 0.04 Å longer than standard uranyl (VI) oxo bond lengths of ~ 1.77 Å).⁴³ The U–O distances for U(V) species are often upward of 1.88 Å,^{7,44} though they have been cited as low as 1.810 Å.^{45,46} For the previously characterized aqua complex, U=O lengths of 1.77(2) and 1.76(2) Å are found; however, the estimated standard deviations (esd) values observed are larger by an order of magnitude.³¹ We attribute this elongation to the noninnocent character of the gbha ligand, which is most evident from the C1–O1 and C114–O102 bond lengths of 1.29(2) Å. The corresponding bonds in $\text{UO}_2\text{-1b}$ retain their phenolate character with lengths of 1.342(18) and 1.350(19) Å as does the C14–O2 bond of $\text{UO}_2\text{-1c}$, whereas these shorter bonds are consistent with a higher bond order, as has previously been observed for systems with this type of quinoid distortion, bearing some similarity to radical anion ligands.^{29,30,47} In unit A (Figure 5), the quinoid-type distortions of the rings can be seen, though they are subtle, especially in comparison to that of $\text{UO}_2\text{-1b}$ and are not significant given the low C–C bond precision of the structure. Additionally, we see differences in the α -diimine fragments of units A and B; most notably, the C107–C108 distance in unit B is shortened to 1.40(2) Å from 1.44(2) Å in unit A and in $\text{UO}_2\text{-1b}$, again consistent with radical-like redistribution of electron density. Despite the esd values being large, this difference is still meaningful as it coincides with some elongation of the average C–N distance to 1.281(19) Å, which is intermediate to the approximately 1.32 Å distance diagnostic of the singly reduced radical anion form and the approximately 1.24 Å distance for neutral gbha species.^{29,42} Interestingly, unit A, which has a very intermediate C7–C8

distance of 1.44(2) Å, has a longer average C–N distance of 1.311(19) Å, which is much more consistent with a reduced bond order than with a typical double bond. The equatorial U–N and U–O bond lengths of 2.558(12) and 2.319(10) are consistent with the assignment of a U(VI) species^{18,48} and suggest the nitrogen is still donating as a neutral atom, not an anionic one, which would be reflected by U–N distances approximately 0.20 Å shorter than those observed.¹⁶ In solution, this species shows no indication of persistent radicals, as the NMR spectra appear typical for diamagnetic complexes, and is EPR silent. We therefore favor assignment of this species as a gbha U(VI) complex which exclusively in the crystalline state has some characteristics of a U(VI) gbha radical. These findings clearly illustrate the noninnocent character of the gbha ligand and its impact on structural features of uranyl complexes.

We also examined the structures of complexes $\text{UO}_2\text{-1e}$ and f , which crystallize as water- and methanol-coordinated monomers, respectively (Figure 6). While there is some deviation from planarity of the ligand in both cases, it is much less significant (7.40° (e), 7.33° (f)) than that in $\text{UO}_2\text{-1b}$ and $\text{UO}_2\text{-1c}$. $\text{UO}_2\text{-1e}$ has average U–N and U–O bond lengths of 2.558(4) and 2.312(4) Å, and those of $\text{UO}_2\text{-1f}$ are 2.546(13) and 2.267(11) Å. These values are consistent with the other species and with the assignment of U(VI) centers. In both cases, the α -diimine fragments bear some radical-type character (C–C: 1.452 (7), C–N: 1.283 (7) for $\text{UO}_2\text{-1e}$; C–C: 1.44(2), C–N: 1.293(8) for $\text{UO}_2\text{-1f}$), but this is not reflected elsewhere in the complexes, perhaps due to the electronegativity of the fluorine and greater degree of delocalization possible for the naphthyl system. The uranyl U=O bond lengths for both of these species only show very small variations: for $\text{UO}_2\text{-1e}$, 1.779(5) (U1–O3) and 1.791(5) (U1–O4), and for $\text{UO}_2\text{-1f}$, 1.770(11) (U1–O3) and 1.785(11) (U1–O4). We do note that although this lengthening of the U1–O4 for the naphthyl complex ($\text{UO}_2\text{-1e}$) is rather small and is in fact statistically insignificant, it is of interest as O3 engages in several long-range, weak contacts to H atoms in a “proton pocket”, including to the interstitial benzene H1S shown in Figures 5

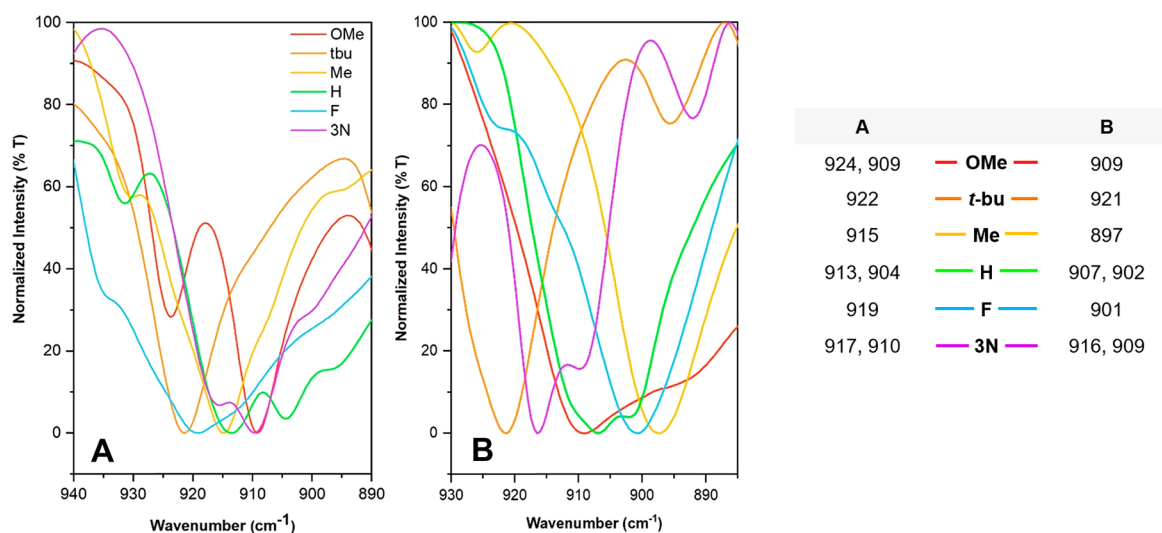


Figure 7. Uranyl U=O asymmetric (ν_3) stretches for gbha complexes (A) and phen-BIAN complexes (B) and table of vibrational frequencies (cm^{-1}).

and S41 (2.784 Å). Generally, an increase in bond length would be expected for the oxo ligand engaging in contacts with electropositive species,⁴⁹ not the oxo ligand *trans* to it; however, we have observed this slight “asymmetry” previously where uranyl–solvent interactions are present.²⁵ The latter, more predictable behavior is observed for $\text{UO}_2\text{-1e}$, where O4 engages in a greater number of weak H atom interactions (Figure S40).

Infrared Spectroscopy. To gain better insight into how the equatorial ligand electronics impact the uranyl moiety, the vibrational properties of complexes $\text{UO}_2\text{-1a-f}$ and $\text{UO}_2\text{-2a-f}$ were characterized using infrared spectroscopy. The symmetric (ν_1 , Raman active) and asymmetric (ν_3 , IR active) vibrational modes are characteristic of the uranyl moiety,^{50–52} making vibrational spectroscopy a useful probe to evaluate ligand influence on axial interactions. It has been well-established that uranyl stretching frequencies are strongly indicative of the binding strength of the equatorial ligands and can therefore serve as a measure of covalency.^{53–55} The large assembly of compounds presented herein represents a unique opportunity to examine the impacts of both R-group substitution and degree of ligand conjugation on the axial-yl interactions. The IR spectra featuring the ν_3 stretches of the two sets of uranyl complexes (gbha and phen-BIAN) are shown in Figure 7.

While no trends are obvious at first glance other than the *t*-bu-substituted complex having the highest frequency in both cases, on closer inspection, several features become apparent. First, as the phen-BIAN complexes show a greater variation in their ν_3 values and are overall lower in energy by an average of 8.4 cm^{-1} than those of the gbha complexes, it is notable that for most cases, the values are closely matched. The exceptions here are the F- (901 cm^{-1}) and Me-phen-BIAN (897 cm^{-1}) complexes (Figure 7), indicating that the presence of electron-donating groups *para* to the imine N in conjunction with the extended π -system offered by the acenaphthene backbone affords a unique ligand environment that is more strongly donating and thus possessing of somewhat greater covalent character than its gbha counterparts.⁵³ The electron-donating effects of these substituents can also be observed in the N–H stretching frequencies of the gbha ligands as benzoxazinobenzoxazines (Figure S33). Second, the presence of an electron-

donating substituent *para* to the phenolic donor does not have the same effect on the ν_3 O=U=O stretch. In fact, these complexes (OMe, *t*-bu) generally have the highest stretching frequencies. While these substituents should increase the electron density of the phenolic donor, this behavior is not necessarily reflected in the IR data; rather, the concomitant decrease of electron density at the imine N may be reflected here. In the case of the phen-BIAN complexes, these data implicate a greater covalent contribution from the imine N atoms than the phenolic oxygens. This is curious, given the π -accepting nature of the α -diimine fragment, and the unambiguous retention of the electron-deficient U(VI) oxidation state.

For those species that exhibit two ν_3 stretching frequencies, we attribute this splitting to the asymmetry of the U=O bonds. For the unsubstituted gbha complex $\text{UO}_2\text{-1c}$, the presence of two stretching frequencies at 913 and 904 cm^{-1} is consistent with its solid-state structure, where the latter corresponds to the elongated U=O bond ($1.809(9) \text{ \AA}$). $\text{UO}_2\text{-1f}$ also exhibits elongation of one of the U=O bonds to a lesser extent, but this asymmetry is still reflected by the IR data. No new crystal structures of the phen-BIAN complexes could be obtained due in large part to their poor solubility, but these data indicate that both $\text{UO}_2\text{-2c}$ (-H) and $\text{UO}_2\text{-2f}$ (-3N) may also show perturbations of the oxo bonds.

Electronic Spectroscopy. The absorption spectra of the UO_2 -gbha complexes is shown in Figure 8. These spectra generally feature two primary intense absorption bands at $366\text{--}388 \text{ nm}$ ($\sim 5400\text{--}9600 \text{ M}^{-1} \text{ cm}^{-1}$) and $578\text{--}712 \text{ nm}$ ($9400\text{--}13\,500 \text{ M}^{-1} \text{ cm}^{-1}$) attributed to $\pi \rightarrow \pi^*$ transitions between the phenolic donors and the α -diimine moiety and the formation of phenoxyl radicals, respectively.^{29,56} The lower-energy transitions are of intraligand charge transfer (ILCT) type and arise due to the presence of phenolic donors and a π -acceptor unit within the same framework.⁵⁷ The uranyl naphthyl-gbha complex ($\text{UO}_2\text{-1f}$) behaves similarly but is somewhat of an exception: the higher-energy $\pi \rightarrow \pi^*$ transition occurs at 481 nm ($12\,300 \text{ M}^{-1} \text{ cm}^{-1}$), and the lower-energy band at 620 nm is much broader and less intense ($3200 \text{ M}^{-1} \text{ cm}^{-1}$). We can attribute this at least in part to some included free ligand in solution as the ligand and complex

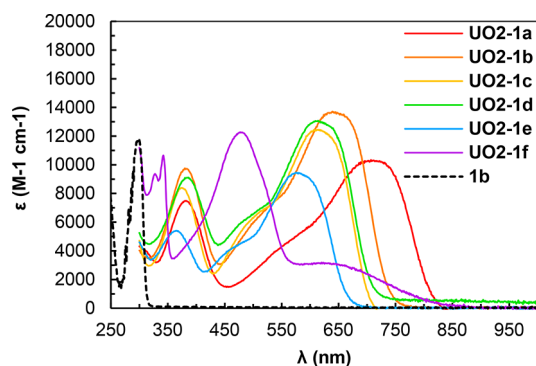


Figure 8. UV-vis data for uranyl-gbha complexes ($\text{UO}_2\text{-1a-f}$), 20 μM in THF. Representative free ligand trace shown for comparison as a dashed line (tbu-gbha (**1b**), 40 μM in THF). The $\text{UO}_2\text{-1f}$ complex includes some free ligand component.

components were inseparable, and therefore, we do not assign much weight to these data, despite it approximately matching the behavior of $\text{UO}_2\text{-2f}$. Shoulders at $\sim 450\text{--}520$ nm are also observed in the spectra of each of the uranyl complexes. These high-intensity ligand features unfortunately preclude any observation of the weak oxo \rightarrow U(VI) LMCT.

It is clear that the primary CT bands for these complexes are ligand-based: when **1b** is dissolved in methanol, the resulting solution is lavender in color, and in addition to the primary absorption at 296 nm, the solution exhibits 2 bands at 365 nm ($380 \text{ M}^{-1} \text{ cm}^{-1}$) and 584 nm ($530 \text{ M}^{-1} \text{ cm}^{-1}$) and a shoulder at ~ 480 nm (Figures S34 and S35). Other ligand derivatives were not investigated for this behavior, as only the *t*-bu derivative has the requisite solubility in room-temperature methanol solutions. In THF and CH_3CN , **1b** as well as the other gbha derivatives are clear and colorless (or very pale yellow). As ILCT processes typically exhibit solvent-polarity dependence,⁵⁷ we sought a route to further confirm this assignment. The closed-shell Zn(II) complex of **1b** was synthesized and studied by UV-vis in several solvents (Figure S35). This complex is solvatochromic and exhibits the same general absorption profile as the free ligand (MeOH) and the uranyl gbha complexes. On the basis of these data, these CT bands can unambiguously be assigned to ligand-based ILCT processes.

Characterization of the $\text{UO}_2\text{-phen-BIAN}$ complexes using UV-vis spectroscopy (Figure 9) revealed similar features to those of the gbha complexes with several key distinctions. First,

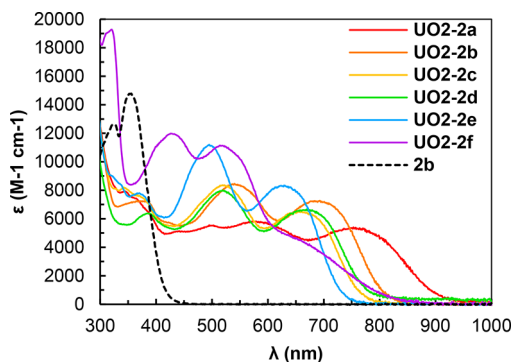


Figure 9. UV-vis data for uranyl-phen-BIAN complexes ($\text{UO}_2\text{-2a-f}$), 20 μM in THF. Representative free ligand trace shown for comparison as dashed line (tbu-phenBIAN, 40 μM in THF).

the energies of λ_{max}^1 are lower in energy by an average of 0.14 eV (+45 nm), as are those of λ_{max}^2 (by ~ 0.06 eV, ~ 20 nm), which can be attributed to the presence of the extended π -system of the acenaphthene unit. Second, the more significant energy-lowering of the λ_{max}^1 CT band relative to that of λ_{max}^2 allows for better resolution of the second CT process. Rather than appearing as shoulders in the gbha complexes, these peaks are distinct, and as in the case of the gbha complexes, can be assigned to ILCT-type transitions. The high-energy bands (λ_{max}^3) are again characteristic of the formation of phenoxyl radicals.^{29,56} Interestingly, the molar absorptivities of these complexes are overall significantly lower than those of the gbha complexes, particularly in the visible region. This is surprising given that these species are more highly conjugated, though a significant difference can be seen between the naphthyl derivative and the others in this respect (Figure 9), especially at lower wavelengths. $\text{UO}_2\text{-2e}$ also has higher molar absorptivities for both CT bands, in contrast to the $\text{UO}_2\text{-1e}$ complex, which has the lowest overall values for ϵ , indicating that different interactions with the ligand backbone are taking place for these two ligand sets. Additionally, the presence of the BIAN backbone allows for better “tuning” of the longest-wavelength ILCT energy, as these peaks occur over a wider range of energies with greater variance among them.

For both the uranyl gbha and uranyl phen-BIAN complexes, a notable trend emerges that those bearing more strongly electron-donating groups have lower-energy absorptions with the methoxy (**1a**, **2a**) derivative being the most strongly donating to the *para* position (in this case the phenolic donor) and having by far the highest λ_{max}^1 value. The λ_{max}^1 values of the *t*-bu, -Me, and -H (unsubstituted) complexes are intermediate, and the -F derivative is lowest. This behavior is consistent with the relative donor strengths of the substituents and their positions relative to the phenolic donor. In both cases, the naphthyl-substituted complex features a broad, less-intense λ_{max}^1 absorption that may result from greater delocalization of charge. These data are summarized in Tables 1 and 2.

Table 1. λ_{max} Values and Extinction Coefficients of Uranyl Gbha Complexes $\text{UO}_2\text{-1a-f}^a$

$\text{UO}_2\text{-1}$ complex	λ_{max}^1 (nm)	λ_{max}^2 (nm)	λ_{max}^3 (nm)
OMe	709 (10 300)	$\sim 550^b$	382 (7500)
<i>t</i> -bu	648 (13 600)	$\sim 525^b$	380 (9800)
Me	614 (13 100)	$\sim 510^b$	388 (9000)
H	613 (12 400)	$\sim 500^b$	375 (8400)
F	575 (9500)	$\sim 470^b$	366 (5400)
3N	620 (~ 3100)	— ^c	481 (12 300)

^aItalicized values are extinction coefficients ($\text{M}^{-1} \text{ cm}^{-1}$). ^bShoulder-estimated λ_{max} 3500–7000 $\text{M}^{-1} \text{ cm}^{-1}$. ^cObscured.

To further elucidate the electronic structure of these ligand systems and corroborate the trend observed experimentally, a series of qualitative calculations was performed on **1a-f**. Because the free ligands exist as cyclic benzoxazinobenzoxazines that lack the α -diimine unit, the open, or “bound” configurations of the of the ligands as diphenolate Schiff bases were modeled. Calculated energies of the longest wavelength ILCT for **1a-e** are on average 0.191 eV higher (57.4 nm lower) than those determined experimentally for their complexes (Table 3), which is nonetheless a good fit despite excluding the uranyl center from the calculations. The

Table 2. λ_{\max} Values and Extinction Coefficients of Uranyl Phen-BIAN Complexes $\text{UO}_2\text{-2a-f}^a$

$\text{UO}_2\text{-2}$ complex	λ_{\max}^1 (nm)	λ_{\max}^2 (nm)	λ_{\max}^3 (nm)
OMe	753 (5400)	578 (5800)	
<i>t</i> -bu	693 (7300)	540 (8500)	381 (7200)
Me	674 (6600)	519 (8000)	386 (6400)
H	660 (6500)	519 (8500)	370 (7600)
F	629 (8300)	495 (11 200)	370 (7800)
3N	$\sim 640^b$	514 (11 100)	426 (12 000)

^aItalicized values are extinction coefficients ($\text{M}^{-1} \text{cm}^{-1}$). ^bExtinction coefficient approximately 4600–4900 $\text{M}^{-1} \text{cm}^{-1}$.

Table 3. Calculated and Experimental Values for Lowest-Energy ILCT Processes (gbha Ligands)

1	calculated λ_{\max}	experimental λ_{\max}^1 ($\text{UO}_2\text{-L}$)	difference	
			nm	eV
OMe (a)	621	709	−88	−0.248
<i>t</i> -bu (b)	575	648	−73	−0.245
Me (d)	563	614	−51	−0.182
H (c)	570	613	−43	−0.152
F (e)	543	575	−32	−0.128
3N (f)	686	620	+66	+0.193

calculated ILCT energies for λ_{\max}^1 match very well with the observed trend for these species, in which complexes of ligands bearing more electron-donating substituents have lower-energy ILCTs. A similar, yet less consistent trend is observed for the λ_{\max}^2 values, and these processes can also be assigned as ILCT-type transitions ($\text{HOMO}-1 \rightarrow \text{LUMO}$).

Though the predicted ILCT energies (λ_{\max}^1) support the experimental data for $\text{UO}_2\text{-1a-e}$, that of the naphthyl-gbha ligand (**1f**) is 0.193 eV lower (66 nm higher) than the experimentally observed value ($\lambda_{\max}^1, \text{calc} = 686 \text{ nm}$; $\lambda_{\max}^1, \text{obs} = 620 \text{ nm}$) for the complex, which deviates substantially from the trend exhibited by the rest of the data. The presence of some free ligand in solution may be a complicating factor. It is unsurprising that the predicted energy of this ILCT is lower than those for the other ligands given the presence of the extended π -system; however, the discrepancy between this and the experimentally determined ILCT energy warrants further investigation. While the greater degree of delocalization is most likely implicated here, this deviation could also indicate the presence of more complicated metal–ligand interactions that

may increase the energy required to transfer additional charge to the diimine LUMO. There are other possible sources for this behavior. The solid-state structure of this species does show a slight twist of the ligand, and in solution, two distinct peaks are observed by ^1H NMR that can be assigned to two imine protons in different environments. These protons are not observed for the free ligand. If the naphthyl rings are distorted significantly out of plane in solution, this CT process would likely be higher in energy, and this would account for the low intensity of the band. Similar spectroscopic behavior is observed for $\text{UO}_2\text{-2f}$, which also features extended conjugation. Especially considering recent work highlighting backbonding interactions between an electron-poor uranium center and a poor π -acceptor in the presence of suitable ancillary ligands,²¹ we do entertain the idea that ligand environments such as those of **1f** and **2f** which provide large, accessible π -systems may be sufficiently π -accepting to participate in similar bonding interactions, even with U(VI). Given that the electron density necessary for metal back-donation to the diimine unit could be supplied by the phenolic donors, as has been observed previously in d^0 transition metal complexes,⁵⁸ this is worth investigating in further studies.

Electrochemistry. Electrochemical studies of the uranyl gbha complexes were carried out to further characterize the electronic effects of ligand substitution on the uranyl center. Due to poor solubility of many of the complexes, quality electrochemical data could not be obtained for all derivatives. The electrochemical behavior of these species is also highly solvent-dependent (Figure S43). For the $\text{UO}_2\text{-L1b}$ and **c**, a fairly complex electrochemical profile is observed (Figure 10), featuring multiple metal-centered redox events and indicating that these species exist as dimers in solution. $\text{UO}_2\text{-1d-e}$ (−Me and −F derivatives), however, each exhibit only one distinct peak that can be attributed to a metal-centered process (Figure S44), suggesting that these complexes are most likely monomeric in solution. These three species all bear substituents that are ortho/para-directors and remove electron density from the phenolic carbon (Me, F), or delocalize electron density over the entire arm (3N), which should disfavor the μ -phenolato bridged dimers observed for *t*-tbu and −H-substituted complexes in the solution state.

$\text{UO}_2\text{-1b}$ and $\text{UO}_2\text{-1c}$ feature multiple sequential redox events with those of $\text{UO}_2\text{-1b}$ occurring at potentials 40–50 mV more negative than those of $\text{UO}_2\text{-1c}$, which is expected based on the presence of the electron-donating *t*-bu group. Processes 1, 2, and 3 occur at −1.11 V ($\Delta E = 68 \text{ mV}$), −1.32 V

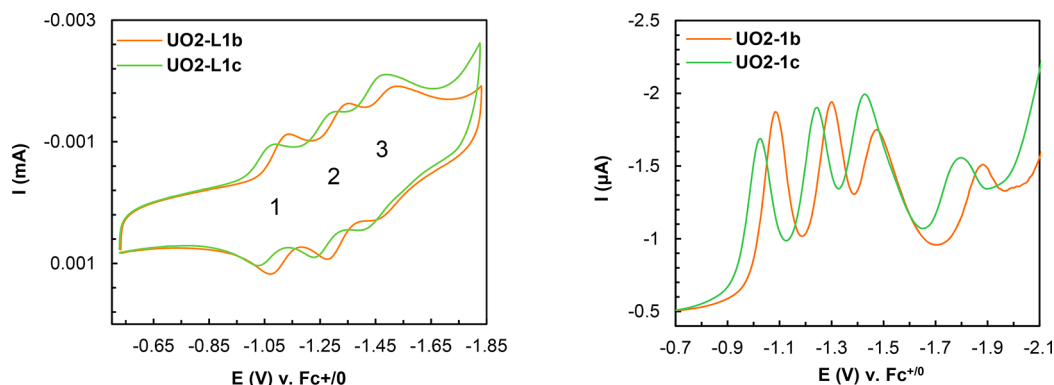


Figure 10. CV (left) and DPV (right) of uranyl complexes, 100 μM in CH_2Cl_2 . WE: glassy carbon; CE: Pt wire; WE: Ag/AgCl, sat'd. KCl/ H_2O . CV: 0.1 V/s.

($\Delta E = 75$ mV), and -1.48 V ($\Delta E = 102$ mV) for **UO₂-1b** and -1.06 V ($\Delta E = 64$ mV), -1.27 V ($\Delta E = 84$ mV), and -1.44 V ($\Delta E = 104$ mV) for **UO₂-1c**, respectively. In both cases, processes 1 and 2 are reversible (or nearly reversible), and process 3 is quasireversible. This behavior is similar to that previously observed for [UO₂(*t*-bu)phen-BIAN]₂ (**UO₂-2b**), which was determined to undergo reduction from [U^{VI}–U^{VI}] to [U^{IV}–U^{IV}] through a series of mixed-valent states.²² The UO₂^{2+/+} (U^{VI/V}) redox couple is highly dependent on the nature of the equatorial ligand and can range from -1.1 to -1.8 V (vs Fc^{+/0}).^{5,45} While the values for processes 1–3 are consistent with one-electron reductions of dimeric uranyl species as previously observed, the formation of ligand-centered radicals and retention of the U^{VI} center or formation of U^{VI}–U^V ligand radicals is also probable, as these ligands are noninnocent, and we determined from the solid-state structures of **UO₂-1b** and **UO₂-1c** that the (*t*-bu)gbha and gbha ligands already possess some radical-anion-like characteristics.¹⁸ We do favor the former assignment, as electrochemical behavior is strongly solvent-dependent, and reductions at -1.80 V (**UO₂-1c**) and -1.87 V (**UO₂-1b**) consistent with reduction of the diimine^{59–61} are observed in the DPVs of the complexes. This feature is mostly obscured in a large increase in current in CV experiments, and once this reduction occurs, the reductive behavior between -1.0 and -1.7 V is drastically altered in repeated scans (Figure S45). Regardless of the nature of these processes, it is clear that the noninnocence of these α -diimine frameworks affords access to reduced metal oxidation states or their radical anion equivalents. The redox features presented here in context with similar literature speak to there being a wealth of intricacies concerning the interaction of uranyl with noninnocent ligands that have yet to be completely resolved.^{5,15,18,59}

Of note in our evaluation of the impacts of ligand conjugation is the difference in reduction potentials of the *t*-bu-derivatives, **UO₂-1b** and **UO₂-2b**. For the first three processes, those of **UO₂-2b** are consistently 40 mV less negative than those of **UO₂-1b** (Table 4). Also, for **UO₂-2b**, an

Table 4. Redox Processes (DPV) vs Fc^{+/0}

process	UO ₂ -1b (V)	UO ₂ -2b ²² (V)
1	-1.08	-1.04
2	-1.26	-1.20^*
3	-1.42	$-1.38, -1.49$
4		-1.72
5	-1.87	-1.99

*Previously unassigned.

additional shoulder and distinct reduction are observed. From this, it is clear that the large accessible π -system offered by the phen-BIAN framework effectively lowers the reduction potentials as well as provides additional opportunity for reduction of the entire complex by acting as reservoir that electrons can be easily shuttled in to and out of. This demonstrated significant utility over its gbha counterpart with respect to the possibility of stabilizing lower formal oxidation state uranium centers.

CONCLUSIONS

Here, we presented a series of uranyl complexes of substituted α -diimine ligands (gbha and phen-BIAN) in an effort to both compare the effects of aryl group substitution and the presence

of extended π -systems on the behavior of the axial oxo moieties. These ligands contain the π -accepting N=C–C=N fragment and donor phenolic groups that result in the absorption spectra of their complexes being dominated by intense intraligand charge transfer (ILCT) processes. DFT calculations for the gbha complexes support this assignment and agree with the experimentally observed trend in energies as they depend on the electron-donating ability of the aryl substituent, though a deviation in this trend is observed for **UO₂-1f**. Despite the poor solubility of some of these complexes which complicated their characterization, we were able to obtain crystal structures for **UO₂-1b**, **UO₂-1c**, and **UO₂-1f**, showing that these species can form μ -phenolato-bridged dimers, as we have previously observed for **UO₂-2b**,²² or methanol-coordinated monomers. The nuclearity and solvent coordination are solvent-dependent and therefore highly dependent on solubility and crystallization conditions; thus, the solution-state and solid-state structures are not necessarily consistent. These α -diimine ligands behave noninnocently when coordinated to uranyl, as observed for **UO₂-1c**, though we do not observe this species behaving as a U(V) equivalent. Electrochemically, the noninnocence of these systems manifests as multiple redox-processes and allows significant reduction of the complexes. It is not clear if these are strictly ligand-based processes or if the metal centers are primarily involved; rather, these reductions likely correspond to significant delocalization of charge throughout the entire species. We thus conclude that the inclusion of the conjugated BIAN backbone is advantageous as it lowers the overall reduction potentials and allows for a greater number of reductions as observed in our comparison of **UO₂-1b** and **UO₂-2b**. FT-IR analysis of all complexes shows slightly lower ν_3 O=U=O stretching frequencies overall for the **UO₂-2** complexes (phen-BIAN), indicating slight contribution of the more highly conjugated ligand in impacting this axial feature. **UO₂-2d** and **UO₂-2e**, which bear methyl and fluoro substituents *para* to the imine nitrogen, also have significantly lower stretching frequencies (18 cm⁻¹) than their gbha counterparts (**UO₂-1d** and **e**). This not only demonstrates that the combination of an electron-donating group in this position and the BIAN backbone creates a unique electronic environment that more drastically impacts the covalent character of the oxo ligands but also implicates the nitrogen donors as greater contributors to this environment than the phenolic oxygen atoms.

ASSOCIATED CONTENT

Supporting Information

The Supporting Information is available free of charge on the ACS Publications website at DOI: 10.1021/acs.inorgchem.9b01695.

NMR and additional FT-IR and UV–vis spectra, single-crystal X-ray diffraction tables and figures, computational details, and additional electrochemical data (PDF)

Accession Codes

CCDC 1918535, 1918539–1918541, and 1921460 contain the supplementary crystallographic data for this paper. These data can be obtained free of charge via www.ccdc.cam.ac.uk/data_request/cif, by emailing data_request@ccdc.cam.ac.uk, or by contacting The Cambridge Crystallographic Data Centre, 12 Union Road, Cambridge CB2 1EZ, UK; fax: +44 1223 336033.

AUTHOR INFORMATION

Corresponding Author

*E-mail: anne.gorden@auburn.edu

ORCID

Anne E. V. Gorden: 0000-0001-6623-9880

Notes

The authors declare no competing financial interest.

ACKNOWLEDGMENTS

The authors would like to acknowledge that this work was funded by the United States Department of Energy, Basic Energy Sciences through the Chemical Sciences, Geosciences, and Biosciences (CSGB) subdivision for Heavy Elements Chemistry with Award DE-SC0019177 to Auburn University. In addition, the authors would like to acknowledge funding from Auburn University in the form of an Undergraduate Research Fellowship to K.M.H. and as a Malone-Zallen Graduate Fellowship to J.E.N. We would again like to thank Prof. John D. Gorden for help with X-ray crystallography and many useful discussions. We would also like to thank Prof. Byron Farnum for his assistance and the use of his potentiostat and Ethan Hiti and Patrick Donnan for many helpful discussions and assistance setting up the ligand calculations.

REFERENCES

- (1) Denning, R. G.; Snellgrove, T. R.; Woodward, D. R. The electronic structure of the uranyl ion. *Mol. Phys.* **1979**, *37* (4), 1109–1143.
- (2) Gregson, M.; Lu, E.; Mills, D. P.; Tuna, F.; McInnes, E. J. L.; Hennig, C.; Scheinost, A. C.; McMaster, J.; Lewis, W.; Blake, A. J.; Kerridge, A.; Liddle, S. T. The inverse-trans-influence in tetravalent lanthanide and actinide bis(carbene) complexes. *Nat. Commun.* **2017**, *8*, 14137.
- (3) Tatsumi, K.; Hoffmann, R. Bent cis d0MoO22+ vs. linear trans d0f0 UO22+: a significant role for nonvalence 6p orbitals in uranyl. *Inorg. Chem.* **1980**, *19* (9), 2656–2658.
- (4) Cowie, B. E.; Nichol, G. S.; Love, J. B.; Arnold, P. L. Double uranium oxo cations derived from uranyl by borane or silane reduction. *Chem. Commun.* **2018**, *54* (31), 3839–3842.
- (5) Bell, N. L.; Shaw, B.; Arnold, P. L.; Love, J. B. Uranyl to Uranium(IV) Conversion through Manipulation of Axial and Equatorial Ligands. *J. Am. Chem. Soc.* **2018**, *140* (9), 3378–3384.
- (6) Kiernicki, J. J.; Cladis, D. P.; Fanwick, P. E.; Zeller, M.; Bart, S. C. Synthesis, Characterization, and Stoichiometric U–O Bond Scission in Uranyl Species Supported by Pyridine(diimine) Ligand Radicals. *J. Am. Chem. Soc.* **2015**, *137* (34), 11115–11125.
- (7) Arnold, P. L.; Pécharman, A.-F.; Lord, R. M.; Jones, G. M.; Hollis, E.; Nichol, G. S.; Maron, L.; Fang, J.; Davin, T.; Love, J. B. Control of Oxo-Group Functionalization and Reduction of the Uranyl Ion. *Inorg. Chem.* **2015**, *54* (7), 3702–3710.
- (8) Pedrick, E. A.; Schultz, J. W.; Wu, G.; Mirica, L. M.; Hayton, T. W. Perturbation of the O–U–O Angle in Uranyl by Coordination to a 12-Membered Macrocyclic. *Inorg. Chem.* **2016**, *55* (11), 5693–5701.
- (9) Pedrick, E. A.; Wu, G.; Hayton, T. W. Oxo Ligand Substitution in a Cationic Uranyl Complex: Synergistic Interaction of an Electrophile and a Reductant. *Inorg. Chem.* **2015**, *54* (14), 7038–7044.
- (10) Renshaw, J. C.; Butchins, L. J. C.; Livens, F. R.; May, I.; Charnock, J. M.; Lloyd, J. R. Bioreduction of Uranium: Environmental Implications of a Pentavalent Intermediate. *Environ. Sci. Technol.* **2005**, *39* (15), 5657–5660.
- (11) Korobkov, I.; Gorelsky, S.; Gambarotta, S. Reduced Uranium Complexes: Synthetic and DFT Study of the Role of π Ligation in the Stabilization of Uranium Species in a Formal Low-Valent State. *J. Am. Chem. Soc.* **2009**, *131* (30), 10406–10420.
- (12) Kraft, S. J.; Williams, U. J.; Daly, S. R.; Schelter, E. J.; Kozimor, S. A.; Boland, K. S.; Kikkawa, J. M.; Forrest, W. P.; Christensen, C. N.; Schwarz, D. E.; Fanwick, P. E.; Clark, D. L.; Conradson, S. D.; Bart, S. C. Synthesis, Characterization, and Multielectron Reduction Chemistry of Uranium Supported by Redox-Active α -Diimine Ligands. *Inorg. Chem.* **2011**, *50* (20), 9838–9848.
- (13) Pattenaude, S. A.; Mullane, K. C.; Schelter, E. J.; Ferrier, M. G.; Stein, B. W.; Bone, S. E.; Lezama Pacheco, J. S.; Kozimor, S. A.; Fanwick, P. E.; Zeller, M.; Bart, S. C. Redox-Active vs Redox-Innocent: A Comparison of Uranium Complexes Containing Diamine Ligands. *Inorg. Chem.* **2018**, *57* (11), 6530–6539.
- (14) Li Manni, G.; Walensky, J. R.; Kraft, S. J.; Forrest, W. P.; Pérez, L. M.; Hall, M. B.; Gagliardi, L.; Bart, S. C. Computational Insights into Uranium Complexes Supported by Redox-Active α -Diimine Ligands. *Inorg. Chem.* **2012**, *51* (4), 2058–2064.
- (15) Takao, K.; Tsushima, S.; Ogura, T.; Tsubomura, T.; Ikeda, Y. Experimental and Theoretical Approaches to Redox Innocence of Ligands in Uranyl Complexes: What Is Formal Oxidation State of Uranium in Reductant of Uranyl(VI)? *Inorg. Chem.* **2014**, *53* (11), 5772–5780.
- (16) Anderson, N. H.; Odoh, S. O.; Williams, U. J.; Lewis, A. J.; Wagner, G. L.; Lezama Pacheco, J.; Kozimor, S. A.; Gagliardi, L.; Schelter, E. J.; Bart, S. C. Investigation of the Electronic Ground States for a Reduced Pyridine(diimine) Uranium Series: Evidence for a Ligand Tetraanion Stabilized by a Uranium Dimer. *J. Am. Chem. Soc.* **2015**, *137* (14), 4690–4700.
- (17) Bell, N. L.; Arnold, P. L.; Love, J. B. Controlling uranyl oxo group interactions to group 14 elements using polypyrrolic Schiff-base macrocyclic ligands. *Dalton. Trans.* **2016**, *45* (40), 15902–15909.
- (18) Pankhurst, J. R.; Bell, N. L.; Zegke, M.; Platts, L. N.; Lamfsus, C. A.; Maron, L.; Natrajan, L. S.; Sproules, S.; Arnold, P. L.; Love, J. B. Inner-sphere vs. outer-sphere reduction of uranyl supported by a redox-active, donor-expanded dipyrin. *Chem. Sci.* **2017**, *8* (1), 108–116.
- (19) Lukens, W. W.; Speldrich, M.; Yang, P.; Duignan, T. J.; Autschbach, J.; Kögerler, P. The roles of 4f- and 5f-orbitals in bonding: a magnetochemical, crystal field, density functional theory, and multi-reference wavefunction study. *Dalton. Trans.* **2016**, *45* (28), 11508–11521.
- (20) Fortier, S.; Walensky, J. R.; Wu, G.; Hayton, T. W. High-Valent Uranium Alkyls: Evidence for the Formation of $U^{VI}(CH_2SiMe_3)_6$. *J. Am. Chem. Soc.* **2011**, *133* (30), 11732–11743.
- (21) Lu, E.; Atkinson, B. E.; Wooles, A. J.; Boronski, J. T.; Doyle, L. R.; Tuna, F.; Cryer, J. D.; Cobb, P. J.; Vitorica-Yrezabal, I. J.; Whitehead, G. F. S.; Kaltsoyannis, N.; Liddle, S. T. Back-bonding between an electron-poor, high-oxidation-state metal and poor π -acceptor ligand in a uranium(v)–dinitrogen complex. *Nat. Chem.* **2019**, *11* (9), 806–811.
- (22) Niklas, J. E.; Farnum, B. H.; Gorden, J. D.; Gorden, A. E. V. Structural Characterization and Redox Activity of a Uranyl Dimer and Transition-Metal Complexes of a Tetradentate BIAN Ligand. *Organometallics* **2017**, *36* (23), 4626–4634.
- (23) Fedushkin, I. L.; Skatova, A. A.; Chudakova, V. A.; Fukin, G. K. Four-Step Reduction of dpp-Bian with Sodium Metal: Crystal Structures of the Sodium Salts of the Mono-, Di-, Tri- and Tetraanions of dpp-Bian. *Angew. Chem., Int. Ed.* **2003**, *42* (28), 3294–3298.
- (24) Fedushkin, I. L.; Skatova, A. A.; Chudakova, V. A.; Cherkasov, V. K.; Fukin, G. K.; Lopatin, M. A. Reduction of 1,2-Bis[2,6-diisopropylphenyl]imino]acenaphthene (dpp-Bian) with Alkali Metals – A Study of the Solution Behaviour of $(dpp-Bian)_n-[M^+]_n$ ($M = Li, Na; n = 1-4$) with UV/Vis, ESR and 1H NMR Spectroscopy. *Eur. J. Inorg. Chem.* **2004**, *2004* (2), 388–393.
- (25) Niklas, J. E.; Hardy, E. E.; Gorden, A. E. V. Solid-state structural elucidation and electrochemical analysis of uranyl naphthylsalophen. *Chem. Commun.* **2018**, *54* (83), 11693–11696.
- (26) Milligan, C. W.; Lindstrom, F. Colorimetric determination of calcium using reagents of the glyoxal bis(2-hydroxyanil) class. *Anal. Chem.* **1972**, *44* (11), 1822–1829.

- (27) Wilson, A. D. The use of glyoxal bis-(2-hydroxyanil) in determining microgram amounts of uranium. *Analyst* **1962**, *87* (1038), 703–706.
- (28) Bayer, E. Synthese Makromolekularer Komplexbildner aus Aminophenolen und Glyoxal. *Chem. Ber.* **1957**, *90* (12), 2785–2791.
- (29) Roy, A. S.; Muresan, N.; Tuononen, H. M.; Rath, S. P.; Ghosh, P. Electronic structure of the glyoxalbis(2-hydroxyanil) (gha) ligand in $[\text{Co}^{\text{III}}(\text{gha})(\text{PPh}_3)_2]^+$: radical vs. non-radical states. *Dalton. Trans.* **2008**, No. 26, 3438–3446.
- (30) Min, K. S.; Weyhermüller, T.; Bothe, E.; Wieghardt, K. Tetradentate Bis(o-iminobenzosemiquinonate(1-)) π Radical Ligands and Their o-Aminophenolate(1-) Derivatives in Complexes of Nickel(II), Palladium(II), and Copper(II). *Inorg. Chem.* **2004**, *43* (9), 2922–2931.
- (31) Bandoli, G.; Clemente, D. A. Preparation and crystal structure of aqua[bis(2-hydroxyphenylimino)-ethanato-OO'NN'-]dioxouranium. *J. Chem. Soc., Dalton Trans.* **1975**, *7*, 612–615.
- (32) Tauer, E.; Grellmann, K.-H.; Kaufmann, E.; Noltemeyer, M. The condensation product of 2-aminophenol and glyoxal. Structure and photochemistry. *Chem. Ber.* **1986**, *119* (11), 3316–3325.
- (33) Malek, A.; Fresco, J. M. Formation of New Tetradentate Schiff Base Metal Chelates. *Can. J. Chem.* **1973**, *51* (12), 1981–1989.
- (34) Xiong, D.; Fu, Z.; Zhong, S.; Jiang, X.; Yin, D. Novel homogeneous Salen Mn(III) catalysts synthesized from dialdehyde or diketone with o-aminophenol for catalyzing epoxidation of alkenes. *Catal. Lett.* **2007**, *113* (3), 155–159.
- (35) DOC-M86-EXX229 V1 APEX3 Crystallography Software Suite User Manual. Bruker AXS Inc.: Madison, Wisconsin, 2016.
- (36) Sheldrick, G. M. *Acta Crystallogr., Sect. A: Found. Crystallogr.* **2008**, *A64*, 112.
- (37) Dolomanov, O. V.; Bourhis, L. J.; Gildea, R. J.; Howard, J. A. K.; Puschmann, H. OLEX2: A complete structure solution, refinement and analysis program. *J. Appl. Crystallogr.* **2009**, *42*, 339–341.
- (38) Frisch, M. J.; Trucks, G. W.; Schlegel, H. B.; Scuseria, G. E.; Robb, M. A.; Cheeseman, J. R.; Scalmani, G.; Barone, V.; Petersson, G. A.; Nakatsuji, H.; Li, X.; Caricato, M.; Marenich, A. V.; Bloino, J.; Janesko, B. G.; Gomperts, R.; Mennucci, B.; Hratchian, H. P.; Ortiz, J. V.; Izmaylov, A. F.; Sonnenberg, J. L.; Williams, Ding, F.; Lipparini, F.; Egidi, F.; Goings, B.; Peng, B.; Petrone, A.; Henderson, T.; Ranasinghe, D.; Zakrzewski, V. G.; Gao, J.; Rega, N.; Zheng, G.; Liang, W.; Hada, M.; Ehara, M.; Toyota, K.; Fukuda, R.; Hasegawa, J.; Ishida, M.; Nakajima, T.; Honda, Y.; Kitao, O.; Nakai, H.; Vreven, T.; Throssell, K.; Montgomery, Jr., J. A.; Peralta, J. E.; Ogliaro, F.; Bearpark, M. J.; Heyd, J. J.; Brothers, E. N.; Kudin, K. N.; Staroverov, V. N.; Keith, T. A.; Kobayashi, R.; Normand, J.; Raghavachari, K.; Rendell, A. P.; Burant, J. C.; Iyengar, S. S.; Tomasi, J.; Cossi, M.; Millam, J. M.; Klene, M.; Adamo, C.; Cammi, R.; Ochterski, J. W.; Martin, R. L.; Morokuma, K.; Farkas, O.; Foresman, J. B.; Fox, D. J. *Gaussian 16*, Rev. B.01; Gaussian, Inc.: Wallingford, CT, 2016.
- (39) Avogadro: an open-source molecular builder and visualization tool. Version 1.2.0. <http://avogadro.cc/>.
- (40) Suttill, J. A.; Wasserscheid, P.; McGuinness, D. S.; Gardiner, M. G.; Evans, S. J. A survey of pendant donor-functionalised (N,O) phosphine ligands for Cr-catalysed ethylene tri- and tetramerisation. *Catal. Sci. Technol.* **2014**, *4* (8), 2574–2588.
- (41) Ghosh, P.; Bill, E.; Weyhermüller, T.; Neese, F.; Wieghardt, K. Noninnocence of the Ligand Glyoxal-bis(2-mercaptoanil). The Electronic Structures of $[\text{Fe}(\text{gma})_2]$, $[\text{Fe}(\text{gma})(\text{py})]\text{py}$, $[\text{Fe}(\text{gma})(\text{CN})]1-/0$, $[\text{Fe}(\text{gma})\text{I}]$, and $[\text{Fe}(\text{gma})(\text{PR}_3)_n]$ ($n = 1, 2$). Experimental and Theoretical Evidence for “Excited State” Coordination. *J. Am. Chem. Soc.* **2003**, *125* (5), 1293–1308.
- (42) Gardiner, M. G.; Hanson, G. R.; Henderson, M. J.; Lee, F. C.; Raston, C. L. Paramagnetic Bis(1,4-di-tert-butyl-1,4-diazabutadiene) Adducts of Lithium, Magnesium, and Zinc. *Inorg. Chem.* **1994**, *33* (11), 2456–2461.
- (43) Fortier, S.; Hayton, T. W. Oxo ligand functionalization in the uranyl ion (UO_2^{2+}). *Coord. Chem. Rev.* **2010**, *254* (3), 197–214.
- (44) Arnold, P. L.; Hollis, E.; Nichol, G. S.; Love, J. B.; Griveau, J.-C.; Caciuffo, R.; Magnani, N.; Maron, L.; Castro, L.; Yahia, A.; Odoh, S. O.; Schreckenbach, G. Oxo-Functionalization and Reduction of the Uranyl Ion through Lanthanide-Element Bond Homolysis: Synthetic, Structural, and Bonding Analysis of a Series of Singly Reduced Uranyl–Rare Earth $\text{Sf}1\text{–}4\text{fn}$ Complexes. *J. Am. Chem. Soc.* **2013**, *135* (10), 3841–3854.
- (45) Hayton, T. W.; Wu, G. Synthesis, Characterization, and Reactivity of a Uranyl β -Diketiminato Complex. *J. Am. Chem. Soc.* **2008**, *130* (6), 2005–2014.
- (46) Denning, R. G. Electronic Structure and Bonding in Actinyl Ions and their Analogs. *J. Phys. Chem. A* **2007**, *111* (20), 4125–4143.
- (47) Lu, C. C.; Bill, E.; Weyhermüller, T.; Bothe, E.; Wieghardt, K. The Monoanionic π -Radical Redox State of α -Iminoketones in Bis(ligand)metal Complexes of Nickel and Cobalt. *Inorg. Chem.* **2007**, *46* (19), 7880–7889.
- (48) Hardy, E. E.; Wyss, K. M.; Eddy, M. A.; Gorden, A. E. V. An example of unusual pyridine donor Schiff base uranyl (UO_2^{2+}) complexes. *Chem. Commun.* **2017**, *53* (42), 5718–5720.
- (49) Arnold, P. L.; Pécharman, A.-F.; Hollis, E.; Yahia, A.; Maron, L.; Parsons, S.; Love, J. B. Uranyl oxo activation and functionalization by metal cation coordination. *Nat. Chem.* **2010**, *2* (12), 1056–1061.
- (50) Jones, L. H. Systematics in the vibrational spectra of uranyl complexes. *Spectrochim. Acta* **1958**, *10* (4), 395–403.
- (51) Jones, L. H.; Penneman, R. A. Infrared Spectra and Structure of Uranyl and Transuranium (V) and (VI) Ions in Aqueous Perchloric Acid Solution. *J. Chem. Phys.* **1953**, *21* (3), 542–544.
- (52) Kalaj, M.; Carter, K. P.; Cahill, C. L. Isolating Equatorial and Oxo Based Influences on Uranyl Vibrational Spectroscopy in a Family of Hybrid Materials Featuring Halogen Bonding Interactions with Uranyl Oxo Atoms. *Eur. J. Inorg. Chem.* **2017**, *2017* (40), 4702–4713.
- (53) Di Pietro, P.; Kerridge, A. U–Oyl Stretching Vibrations as a Quantitative Measure of the Equatorial Bond Covalency in Uranyl Complexes: A Quantum-Chemical Investigation. *Inorg. Chem.* **2016**, *55* (2), 573–583.
- (54) Di Pietro, P.; Kerridge, A. Assessing covalency in equatorial U–N bonds: density based measures of bonding in BTP and isoamethyryn complexes of uranyl. *Phys. Chem. Chem. Phys.* **2016**, *18* (25), 16830–16839.
- (55) Syt'ko, V. V.; Kabaeva, E. N. Special Features of the Correlation between the Uranium–Oxygen Interatomic Distances and the Frequencies of the Valence Vibrations of the (UO_2^{2+}) Group in Complex Compounds of Uranyl. *J. Appl. Spectrosc.* **2002**, *69* (4), 566–570.
- (56) Altwicker, E. R. The Chemistry of Stable Phenoxy Radicals. *Chem. Rev.* **1967**, *67* (5), 475–531.
- (57) Benedix, R.; Dietz, F.; Hennig, H. Spectroscopic and theoretical investigations of Schiff base metal complexes with intraligand charge-transfer behavior. *Inorg. Chim. Acta* **1988**, *147* (2), 179–183.
- (58) Lynn, M. A.; Bursten, B. E. An analysis of the bonding in some ‘nonclassical’ d0 and d10 metal carbonyl complexes. *Inorg. Chim. Acta* **1995**, *229* (1), 437–443.
- (59) Viganò, M.; Ferretti, F.; Caselli, A.; Ragaini, F.; Rossi, M.; Mussini, P.; Macchi, P. Easy Entry into Reduced Ar-BIANH2 Compounds: A New Class of Quinone/Hydroquinone-Type Redox-Active Couples with an Easily Tunable Potential. *Chem. - Eur. J.* **2014**, *20* (44), 14451–14464.
- (60) Sondermann, C.; Ringenberg, M. R. Tuning the overpotential of electrocatalytically active cyclopentadienylnickel complexes containing 1,4-diaza-1,3-butadienes (DAB) for proton reduction. *Dalton. Trans.* **2017**, *46* (16), 5143–5146.
- (61) Hasan, K.; Zysman-Colman, E. Synthesis, UV–Vis and CV properties of a structurally related series of bis(Arylimino)-acenaphthenes (Ar-BIANs). *J. Phys. Org. Chem.* **2013**, *26* (3), 274–279.